NANO LETTERS

pubs.acs.org/NanoLett Letter

Manipulation of the van der Waals Magnet $Cr_2Ge_2Te_6$ by Spin–Orbit Torques

Vishakha Gupta, Thow Min Cham, Gregory M. Stiehl, Arnab Bose, Joseph A. Mittelstaedt, Kaifei Kang, Shengwei Jiang, Kin Fai Mak, Jie Shan, Robert A. Buhrman, and Daniel C. Ralph*

Cite This: *Nano Lett.* 2020, 20, 7482–7488 Read Online

ACCESS | Metrics & More | Article Recommendations | Supporting Information

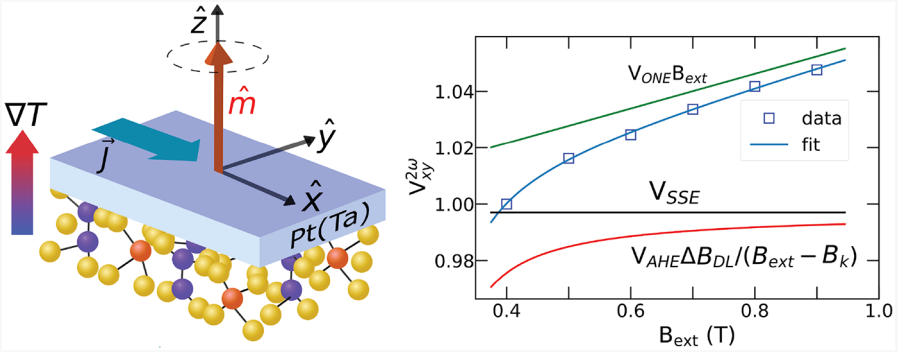

ABSTRACT: We report measurements of current-induced thermoelectric and spin–orbit torque effects within devices in which multilayers of the semiconducting two-dimensional van der Waals magnet $Cr_2Ge_2Te_6$ (CGT) are integrated with Pt and Ta metal overlayers. We show that the magnetic orientation of the CGT can be detected accurately either electrically (using an anomalous Hall effect) or optically (using magnetic circular dichroism) with good consistency. The samples exhibit large thermoelectric effects, but nevertheless, the spin–orbit torque can be measured quantitatively using the angle-dependent second harmonic Hall technique. For CGT/Pt, we measure the spin–orbit torque efficiency to be similar to conventional metallic-ferromagnet/Pt devices with the same Pt resistivity. The interfacial transparency for spin currents is therefore similar in both classes of devices. Our results demonstrate the promise of incorporating semiconducting 2D magnets within spin–orbitronic and magneto-thermal devices.

KEYWORDS: *van der Waals materials, 2D magnets, $Cr_2Ge_2Te_6$, spin–orbit torques, magneto-thermal effects*

INTRODUCTION

The magnetization orientation of magnetic thin films can be manipulated efficiently by spin–orbit torques generated by heavy metals,[1−3] topological insulators,[4−8] and transition metal dichalcogenides.[9−11] The efficiency of these spin–orbit torques can be maximized if the magnetic layer is as thin as possible while maintaining a low magnetic damping, if the saturation magnetization is minimized, and if the magnetic layer has a high electrical resistivity so that current is not wasted by being shunted through the magnetic layer rather than by passing within the spin–orbit layer to generate torque. For all of these reasons, recently discovered semiconducting van der Waals (vdW) magnets[12−14] are promising candidates for improved spin–orbit devices. Additionally, these materials can provide large magnetoresistances for magnetic read-out via spin-filter tunneling,[15−17] and experiments have shown that their magnetic properties can also be tuned by electrical gating,[18] which might be used together with spin–orbit torque to provide added functionality.[19] Initial experiments have been published concerning spin–orbit torque applied by heavy metals to the metallic vdW magnet Fe_3GeTe_2[20,21] and the semiconducting vdW magnet $Cr_2Ge_2Te_6$ (CGT).[22] Here we report additional results on multilayer CGT/Pt and CGT/Ta samples. We demonstrate that the magnetic orientation of the vdW magnet can be detected with good consistency either electrically by an anomalous Hall effect or optically (looking through the heavy-metal layer) by magnetic circular dichroism. We characterize strong magneto-thermoelectric effects in these structures.[23−27] We then provide the first direct quantitative measurement of spin–orbit torque in CGT/Pt, finding a torque efficiency very comparable to those exerted by Pt on conventional 3D metallic ferromagnets. This analysis indicates that the interface transparency for spin currents in CGT/Pt is similar to metallic-ferromagnet/Pt samples and that the

Received: July 17, 2020
Revised: September 24, 2020
Published: September 25, 2020

https://dx.doi.org/10.1021/acs.nanolett.0c02965
Nano Lett. 2020, 20, 7482–7488

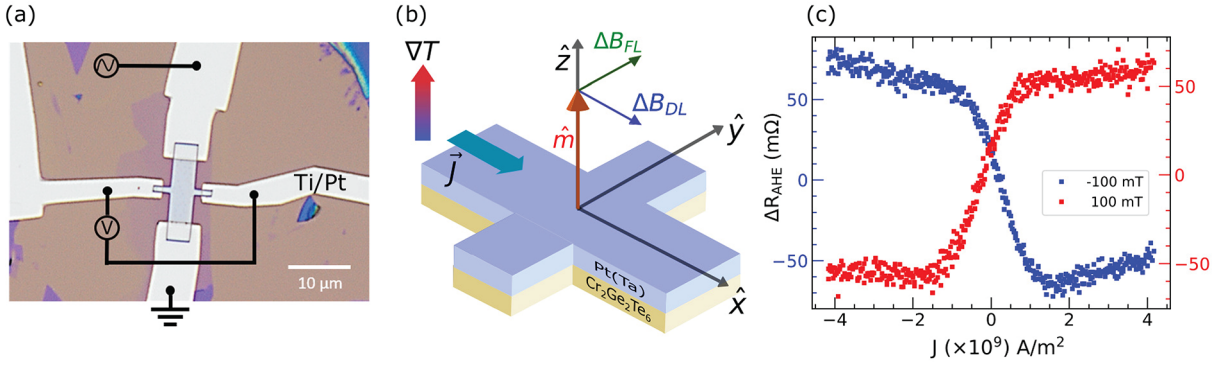

Figure 1. (a) Optical image of a CGT/Pt heterostructure patterned into a Hall bar geometry (4 μm × 11 μm) for transport measurements. (b) Schematic illustrating the orientation of effective fields due to current-induced damping-like torque (ΔB_{DL}) and field-like torque (ΔB_{FL}) acting on the magnetization vector $\vec{m}$. (c) Spin−orbit-torque switching of the magnetization in a CGT(8.9 nm)/Ta(6 nm) sample in the presence of an in-plane field B_x = ±100 mT.

interlayer exchange coupling in multilayer CGT is strong enough that all layers reorient in response to the spin−orbit torque, rather than decoupling.

RESULTS AND DISCUSSION

Device Fabrication. In the bulk, $Cr_2Ge_2Te_6$ is a layered ferromagnetic material with magnetic anisotropy perpendicular to the vdW layers and a Curie temperature of 61 K.[28,29] To fabricate our CGT/Pt and CGT/Ta heterostructures, we first exfoliate multilayers of the 2D magnet from a bulk crystal (HQ graphene) using the scotch tape method on SiO_2 substrates. The exfoliation is done under high vacuum (<10^{-6} Torr) in the load-lock chamber of our sputter system to prevent oxidation of the top surface of the CGT. We then integrate the 2D magnet with the heavy metal (Pt 10 nm or Ta 6 nm) by depositing the metal at a grazing angle (∼5°) by dc magnetron sputtering, to try to minimize damage to the CGT surface. The grazing-angle sputtering results in relatively high resitivities for the heavy-metal films: 1.5 $\mu\Omega$ m for Pt and 3.8 $\mu\Omega$ m for Ta at room temperature. Our procedure differs from the sample fabrication reported in ref 22; in that work, the CGT was exposed to air for a few minutes after exfoliation and was then exposed to an Ar plasma clean before the metal was deposited by conventional sputtering. For our samples, the heavy metal is then coated with 2 nm of Al, which is subsequently oxidized upon exposure to air. We use atomic force microscopy to identify homogeneous regions (with surface roughness <300 pm) on the CGT flakes and pattern them into Hall bars for transport measurements, as shown in Figure 1a. Unless specified otherwise, all measurements were performed at 5 K.

While our fabrication technique works well for CGT, we note that we have also tried with less success to make devices using other vdW magnets. Figure 1 in the Supporting Information shows problems that can arise for $CrBr_3$/Pt and $CrBr_3$/Ta samples.

Detecting the Magnetization State. We find that the magnetization state of CGT/heavy-metal devices can be characterized accurately down to the few-layer limit using either electrical or optical methods.

To electrically characterize the magnetization, one can measure the Hall resistance.[22,30] Figure 2 shows the low-temperature Hall resistance as a function of out-of-plane magnetic field for various thicknesses of CGT and for both Pt and Ta heterostructures. Despite the insulating nature of CGT flakes at temperatures below 100 K,[30] we observe a large

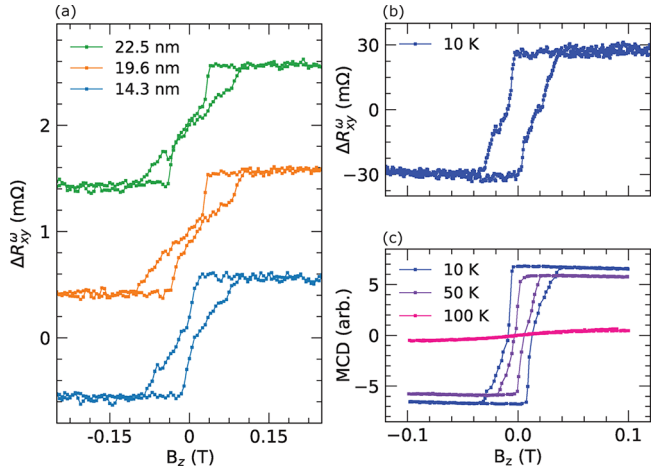

Figure 2. Detecting the magnetization: (a) Anomalous Hall resistance observed in CGT/Pt(10 nm) heterostructures at 5 K, for different CGT thicknesses. (b) Anomalous Hall resistance observed in a CGT(10.5 nm)/Ta(6 nm) sample. (c) Optical MCD detection of magnetization in the same CGT(10.5 nm)/Ta(6 nm) sample at different temperatures.

anomalous Hall signal, similar to the results in refs 22 and 30. This could be due to either a proximity effect in the heavy metal from the adjacent magnet[30] or spin Hall magnetoresistance effects.[31]

It is also possible to use optical measurements to characterize the out-of-plane magnetization, by performing measurements of magnetic circular dichroism (MCD) through the heavy-metal layer. Figure 2c shows magnetic hysteresis curves measured by MCD at various temperatures on the same CGT/Ta sample studied electrically in Figure 2b. We find excellent agreement between the electrical and optical measurements, thus confirming that our anomalous Hall signal is a reliable readout of the sample magnetization, without a major impact on the magnetization state from Ohmic heating. Further, the temperature dependence of the measured anomalous Hall signal in these samples (Figure 3 in the Supporting Information) indicates a Curie temperature that matches well with the bulk value of 61 K.

Spin−Orbit-Torque Switching in CGT/Heavy-Metal Samples. Using the anomalous Hall readout to detect the magnetization state, we demonstrate that current-induced spin−orbit torques in the CGT/heavy-metal samples can

https://dx.doi.org/10.1021/acs.nanolett.0c02965
Nano Lett. 2020, 20, 7482−7488

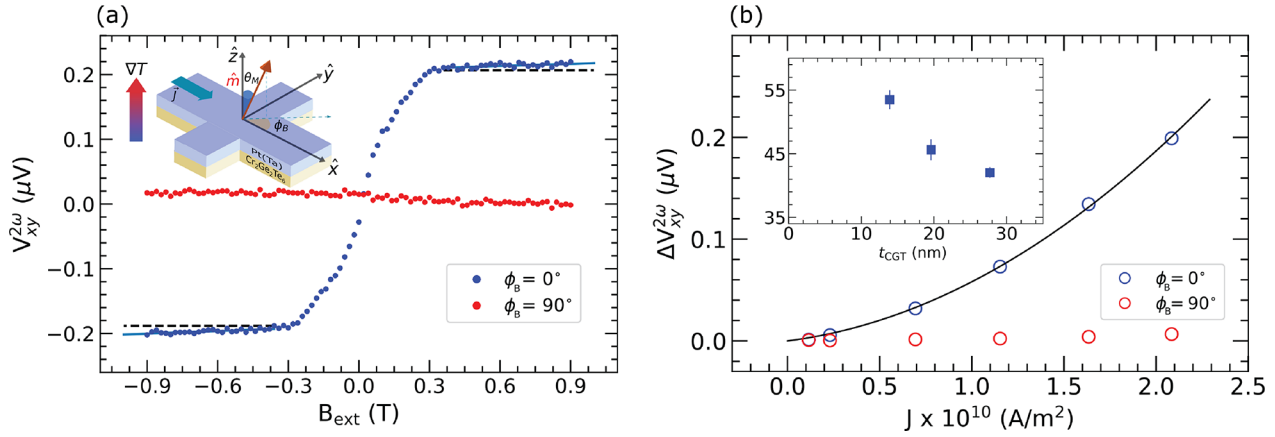

Figure 3. Thermoelectric signals in a CGT(19.6 nm)/Pt(10 nm) sample. (a) Measured $V_{xy}^{2\omega}$ signal at an ac current amplitude of $|\vec{J}| = 2.08 \times 10^{10}$ A/m^2 for external in-plane fields applied along ($\phi_B = 0°$) and perpendicular to the current flow direction ($\phi_B = 90°$). Black dashed lines indicate the value where the signal reaches an approximate plateau after the magnetization is pulled in-plane. Cyan solid lines indicate a small linear background in the signal even after it appears to plateau. (b) Current dependence of the measured SSE signal for both orientations of applied in-plane fields. The black solid line is a parabolic fit. (inset) Magnitude of the parabolic curvature (in units of 10^{-20} nV A^{-2} m^4) for different CGT thicknesses.

switch the perpendicular magnetization of the vdW magnet. Figure 1c shows the measured Hall resistance of a CGT(8.9 nm)/Ta(6 nm) sample while sweeping a dc current applied along $\hat{x}$. In the presence of a constant in-plane magnetic field oriented parallel to $\hat{x}$ that is small compared to the anisotropy field ($B_k \approx 360$ mT, see the Supporting Information) so that it tilts the magnetization into the $\hat{x}$–$\hat{z}$ plane, the magnetic state can be switched between the $+\hat{z}$ and $-\hat{z}$ directions at positive current densities as low as 1.5×10^9 A/m^2 and switched back at negative currents. The polarity of the current-induced switching is inverted on reversing the direction of the in-plane field. These observations are as expected for switching due to a spin–orbit torque[2,32] and confirm the results reported in ref 22. Compared to spin–orbit torque exerted by heavy metals on thin films of 3D ferromagnets with perpendicular magnetic anisotropy,[2,33,34] the critical current densities for switching CGT are smaller by at least an order of magnitude, as one might expect due to the reduced magnetization and coercivity of the CGT films. However, it is difficult to be quantitative about the strength of the spin–orbit torque from such data, because in micron-scale samples spin–orbit-torque switching occurs via a process of domain nucleation and domain-wall motion that is difficult to model in detail.[35] Instead, we use ac-current-driven angle-dependent harmonic Hall measurements to make quantitative estimates of the torques as described below.

Thermoelectric Signals in CGT/Heavy-Metal Devices. Joule heating together with thermoelectric signals in CGT samples[22,24] can produce backgrounds in measurements of spin–orbit torques[36−38] that must be taken into account in order to measure the torques accurately. Similar heating-induced theromelectric signals have been studied previously in heavy-metal/3D ferromagnet samples.[36,38−40] To investigate the coupling of charge, heat, and spin currents in CGT/heavy-metal samples, we inject an ac current $J \| \hat{x}$ and measure the second harmonic Hall voltage $V_{xy}^{2\omega}$ as an external in-plane field changes the orientation of the magnetization vector $\hat{m}$ with respect to the out-of-plane thermal gradient $\nabla T \| \hat{z}$. Figure 3a shows the measured second-harmonic Hall voltage in a CGT(19.6 nm)/Pt(10 nm) sample as a function of in-plane magnetic fields oriented in both the $\hat{x}(\phi_B = 0°)$ and $\hat{y}(\phi_B = 90°)$ directions. Compared to 3D ferromagnet/heavy-metal samples, we observe a thermoelectric signal that is larger relative to the magnetoresistance signals. (This was also noted in ref 22.) For fields along the $\hat{x}$ direction, the signal reaches an approximate plateau at large magnitudes of applied magnetic field where the magnetization is pulled in-plane and the large field strength suppresses the amplitude of precession from current-induced torques. There is a negligible signal when the magnetization is tilted along the $\hat{y}$, perpendicular to the current flow direction. These observations are consistent with the symmetries of the longitudinal spin Seebeck effect (SSE) together with the inverse spin Hall effect in magnetic-insulator/heavy-metal structures[23] where thermally excited magnons induce a spin current in the heavy metal with a flow direction parallel to $\vec{\nabla}T$ that results in a Hall voltage that varies as $\sim \vec{\nabla}T \times \hat{m}$. Further, we measure a positive (negative) $V_{xy}^{2\omega}$ signal when the $\hat{m}$ is along $+\hat{x}(-\hat{x})$, indicating the current-induced $\vec{\nabla}T$ is along $+\hat{z}$, consistent with the expectations from our device geometry.

Consistent with a spin-Seebeck origin, the measured signal scales quadratically with current density $|\vec{J}|$ for fields oriented in the $\hat{x}(\phi_B = 0)$ direction (Figure 3b). The magnitude of the signal decreases with increasing CGT thickness (Figure 3b, inset), suggesting a decreased thermal gradient with increasing thickness. Finally, we note a small linear increase in the $V_{xy}^{2\omega}$ signal with field ($\sim 12 \pm 2$ nV/T), even after the magnetization is saturated in-plane and the signal appears to plateau (Figure 3a). We attribute this to an ordinary Nernst signal that increases linearly with field as $\sim \vec{\nabla}T \times \vec{B}$.[38,41]

Quantifying Spin–Orbit Torques Using Harmonic Hall Measurements. We are now in a position to quantify the strength of spin–orbit torques acting on the 2D magnet, by measuring the second-harmonic Hall response of the sample to an ac current in the presence of an applied external magnetic field of varying magnitude and azimuthal angle.[36−38]

The Hall resistance of the CGT/heavy-metal bilayer in a field regime where a macrospin approximation is accurate can be expressed as

$$R_{xy} = R_{\mathrm{AHE}} \cos\theta_M + R_{\mathrm{PHE}} \sin(2\phi_M) \sin^2\theta_M \qquad (1)$$

where ϕ_M is the azimuthal angle of the magnetization vector $\hat{m}$, θ_M is the polar angle $\hat{m}$ makes with the $\hat{z}$ axis, and R_{AHE} and

https://dx.doi.org/10.1021/acs.nanolett.0c02965
Nano Lett. 2020, 20, 7482−7488

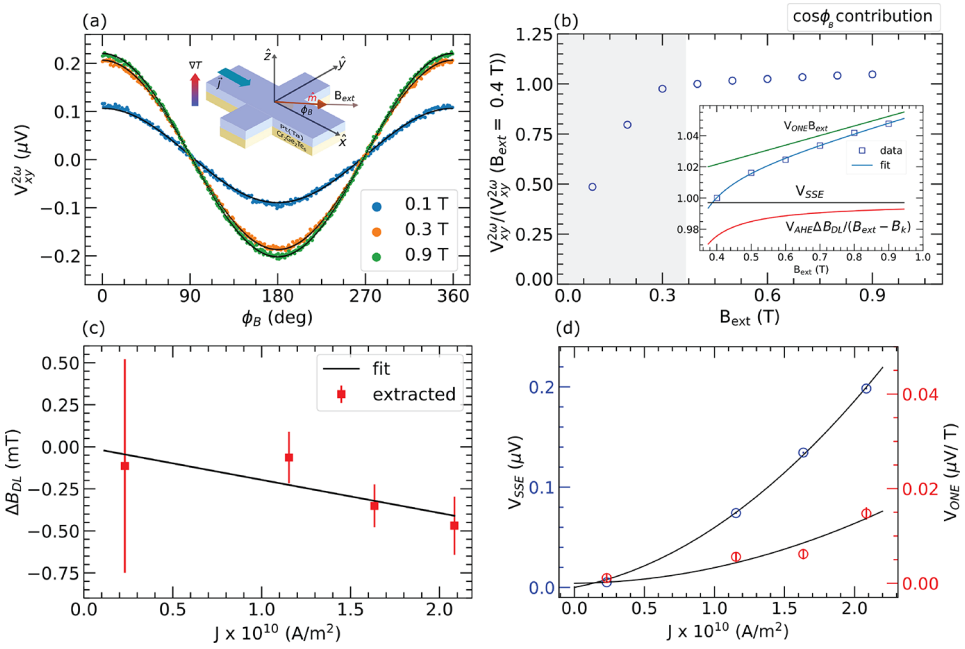

Figure 4. Second-harmonic Hall analysis for CGT(19.6 nm)/Pt(10 nm). (a) Measured $V_{xy}^{2\omega}$ as a function of the azimuthal angle of the applied external field B_{ext}, plotted for different magnitudes of B_{ext}. Solid curves are fits to $\cos\phi_B$. (b) Field dependence of the $\cos\phi_B$ contribution to $V_{xy}^{2\omega}$. The gray region indicates a regime of unsaturated magnetization. (inset) Fit to the $\cos\phi_B$ dependence of $V_{xy}^{2\omega}$, as shown in the saturated regime of the main figure with (black) spin-Seebeck, (green) ordinary Nernst, and (red) damping-like torque contributions. The green and red curves are offset by V_{SSE} for comparison. (c) Current dependence of the effective fields for damping-line torque extracted from the second harmonic signal after subtraction of thermoelectric contributions. The solid line is a straight line fit to the data points. (d) Spin Seebeck and ordinary Nernst contributions extracted from the second harmonic signal. Solid lines are quadratic fits to the data as a function of applied current density.

R_{PHE} are the anomalous Hall and planar Hall resistances of the sample, respectively. When an ac current $\vec{I}(t) = I_0 \sin(\omega t)\hat{x}$ is injected into the sample, the effective fields corresponding to the current-induced damping-like and field-like spin−orbit torques cause periodic oscillations in $\hat{m}$, which lead to oscillations in R_{xy} at frequency ω. The Hall voltage response $V(t) = I(t)R_{xy}(t)$ measured at twice the excitation frequency ($V_{xy}^{2\omega}$) can thus be related to the current-induced effective fields caused by the spin−orbit torques. Additionally, any contributions from Joule-heating-induced thermoelectric effects like the spin Seebeck, anomalous Nernst, and ordinary Nernst effects will also contribute to $V_{xy}^{2\omega}$ but with different dependencies on the magnitude of the externally applied magnetic field (B_{ext}) and the azimuthal angle of the applied field (ϕ_B) that allow them to be separated from the spin−orbit torque signals. Under the assumption that B_{ext} is applied in-plane ($\theta_B = \pi/2$) and is sufficiently large in magnitude to saturate the magnetization along the field direction ($\theta_M = \pi/2$, $\phi_M = \phi_B$), the field and angular dependence of the second harmonic Hall signal can be modeled as[36−38]

$$V_{xy}^{2\omega} = \left(\frac{I_0 R_{AHE}}{2}\frac{\Delta B_{DL}}{B_{ext} - B_k} + V_{ONE}B_{ext} + V_{SSE}\right)\cos(\phi_B) + \left(I_0 R_{PHE}\frac{\Delta B_{FL} + B_{Oe}}{B_{ext}}\right)\cos(2\phi_B)\cos(\phi_B) \quad (2)$$

where ΔB_{DL} is the effective field due to the damping-like torque, B_k is the effective anisotropy field including contributions from both the magnetocrystalline anisotropy and the demagnetizing field ($B_{anis} - B_{demag}$), ΔB_{FL} is the effective field due to the field-like torque, B_{Oe} is the Oersted field generated by the applied current, V_{ONE} is the contribution from the ordinary Nernst effect per unit applied field, and V_{SSE} is the voltage generated due to the spin Seebeck effect. In our measurements, we apply an alternating current density in the range $(1.15-2.08) \times 10^{10}$ A/m^2 at a frequency of 19.7 Hz and an in-plane external field up to 0.9 T utilizing a vector magnet to sweep the angle ϕ_B.

The measured second harmonic Hall voltage $V_{xy}^{2\omega}$ in a CGT(19.6 nm)/Pt(10 nm) sample is plotted in Figure 4a as a function of ϕ_B for different magnitudes of the applied external field. The observed signal fits well to a $\cos\phi_B$ angular dependence (solid curves), indicating a dominant contribution from the ΔB_{DL}, V_{SSE}, and V_{ONE} terms and an almost negligible contribution from $\Delta B_{FL} + B_{Oe}$.

To distinguish the contribution of ΔB_{DL} to $V_{xy}^{2\omega}$ from the thermoelectric signals, for each fixed value of ac current density we consider the dependence of the $\cos\phi_B$ term on the magnitude of the external field B_{ext} (Figure 4b). For fields below the effective anisotropy field in our sample $B_k = 0.36 \pm 0.01$ T (see the Supporting Information), the signal increases sharply as the magnetization gradually rotates toward in-plane (gray region). With increasing magnitude of B_{ext} beyond B_k, the spin-torque-induced oscillations in $\hat{m}$ are gradually suppressed because a given spin−orbit torque produces less magnetization reorientation, whereas the ordinary Nernst contribution increases linearly with B_{ext} and the spin Seebeck term is independent of the applied field magnitude. We observe all three contributions in our measurement. The inset in Figure 4b shows the fit to the $\cos\phi_B$ dependence of $V_{xy}^{2\omega}$ and the individual contributions from ΔB_{DL}, V_{ONE}, and V_{SSE} when $\hat{m}$ is saturated in-plane. The spin Seebeck effect is the largest contribution, consistent with data presented in Figure 3. Both V_{SSE} and V_{ONE} vary quadratically with the applied current density J (Figure 4d), as expected from their thermal origin.

https://dx.doi.org/10.1021/acs.nanolett.0c02965
Nano Lett. 2020, 20, 7482−7488

The effective field from the damping-like torque calculated after subtraction of the thermoelectric contributions to the second harmonic signal is plotted in Figure 4c. We find the magnitude of the damping-like effective field per unit current density to be $|\Delta B_{DL}/J| = (2.0 \pm 0.7) \times 10^{-14}$ T per A m^{-2}.

The corresponding antidamping spin torque efficiency ξ_{DL} per unit current density in the Pt layer can be calculated as

$$\xi_{DL} = \frac{2e}{\hbar}\frac{\Delta B_{DL}}{J} M_s t_{FM} \quad (3)$$

where M_s is the saturation magnetization of CGT and t_{FM} is the CGT thickness. Using the maximum bulk value of the saturation magnetization for CGT ($M_s = 3\ \mu_B$ per Cr atom, or 2.1×10^5 A/m) and the full thickness of the CGT in the sample, we obtain $\xi_{DL} = 0.25 \pm 0.09$. This is very similar to the spin-torque efficiencies for Pt alloys with high resistivities similar to our grazing-angle-sputtered films (1.5 $\mu\Omega$ m) when they act on conventional 3D ferromagnet thin films. For example, PtTi multilayers with similar resistivity act on Co with a spin−orbit-torque efficiency of approximately 0.3.[42] We conclude that the spin−orbit torque efficiency of Pt acting on a vdW magnet is similar to more conventional metallic magnets. We also infer that the magnetization within the full thickness of the CGT layer (19.6 nm ≈ 29 monolayers) responds to the spin−orbit torque. We had wondered, since the interlayer exchange interaction in vdW magnets can be much weaker than the intralayer exchange, whether under the influence of an interfacial spin−orbit torque, the monolayer nearest the interface might decouple and reorient to much larger angles than the bulk of the CGT. However, if this were the case, the apparent spin−orbit torque calculated using eq 3 would be much larger than that for the action of the spin Hall effect of Pt on conventional 3D metallic magnets, and this is not what we observe.

In previous work, ref 22 used a current-induced shift in the magnetic coercivity of a CGT(8 nm)/Ta(5 nm) sample to estimate a value for ΔB_{DL} 40 times larger than our result. This is a much larger difference from our value than would be expected due to the differences in CGT thickness and the spin-torque efficiency of Ta. We suggest that the estimation method used in ref 22 may not be accurate because a damping-like spin−orbit torque might not act on the spatially inhomogeneous magnetic state near coercivity in a way that is equivalent to a simple vertically applied magnetic field. In contrast, a previous measurement of spin−orbit-torque efficiency acting on the metallic 2D ferromagnet Fe_3GeTe_2 is consistent with our results: ref 20 used a measurement technique similar to ours and found a lower bound $\xi_{DL} = 0.14 \pm 0.01$ using a Pt film with resistivity 0.3 $\mu\Omega$ m (consistent with the dependence on Pt resistivity expected from ref 42). In disagreement with ref 20, ref 21 extracted a much larger effective damping-like spin−orbit effective field, $|\Delta B_{DL}/J| = 53.4 \times 10^{-14}$ T per A m^{-2} in a Fe_3GeTe_2 (4 nm)/Pt (6 nm) sample, using a second-harmonic Hall technique with small values of applied in-plane field so that the magnetization remained nearly out-of-plane. We note that the possibility of a contribution from the ordinary Nernst effect was not considered when subtracting thermoelectric signals in that work, and we suspect that this might have affected the result.

Compared to previous angle-dependent second-harmonic Hall measurements on insulating-oxide-ferrimagnet/Pt structures, our measured spin-torque efficiency for CGT/Pt is generally significantly larger; e.g., measurements by different groups on $Tm_3Fe_5O_{12}$/Pt have found $\xi_{DL} \approx 0.014$[31] and $\xi_{DL} = 0.058$,[43] while $\xi_{DL} \approx 0.024$[44] has been reported for $Y_3Fe_5O_{12}$/Pt bilayers. This suggests that the interfacial spin-current transparency is higher in CGT/Pt relative to the oxide-ferrimagnet/Pt structures.

Summary and Outlook. The primary results of this study are as follows: The magnetization configuration within CGT/heavy-metal structures can be characterized down to the few-layer limit using either anomalous Hall measurements or optical magnetic circular dichroism measurements, with good consistency. The strength of thermoelectric signals in these structures can be large relative to magnetoresistance signals, with both the longitudinal spin Seebeck effect and the ordinary Nernst effect contributing measurably to second-harmonic Hall experiments. The large spin Seebeck signals suggest that CGT/heavy-metal samples may be promising systems to investigate magnon dynamics and magnon transport in vdW magnetic materials. Despite the strong thermoelectric signals, angle-dependent second harmonic Hall measurements allow quantitative measurements of the spin−orbit torque exerted by the heavy metal. For CGT/Pt, we find a damping-like spin−orbit torque efficiency of $\xi_{DL} = 0.25 \pm 0.09$ (for a Pt resistivity of 1.5 $\mu\Omega$ m). This value is very similar to previous measurements of spin−orbit torque from Pt acting on conventional metallic magnets but significantly larger than those for the oxide ferrimagnets $Tm_3Fe_5O_{12}$ and $Y_3Fe_5O_{12}$/Pt. This suggests that the interface transparency for spin currents is similar in CGT/Pt and metallic-magnet/Pt structures and higher than that for the oxide-ferrimagnet/Pt interfaces.

■ ASSOCIATED CONTENT

Supporting Information

The Supporting Information is available free of charge at https://pubs.acs.org/doi/10.1021/acs.nanolett.0c02965.

Additional experimental details and discussion, information on the fabrication of $CrBr_3$/Ta and $CrBr_3$/Pt heterostructures, temperature dependence of the anomalous Hall signal in CGT/Pt, and estimation of the effective anisotropy field for CGT/Pt (PDF)

■ AUTHOR INFORMATION

Corresponding Author

Daniel C. Ralph − *Cornell University, Ithaca, New York 14850, United States; Kavli Institute at Cornell, Ithaca, New York 14853, United States*; Email: dcr14@cornell.edu

Authors

Vishakha Gupta − *Cornell University, Ithaca, New York 14850, United States*

Thow Min Cham − *Cornell University, Ithaca, New York 14850, United States*

Gregory M. Stiehl − *Cornell University, Ithaca, New York 14850, United States*

Arnab Bose − *Cornell University, Ithaca, New York 14850, United States*; orcid.org/0000-0003-4696-3112

Joseph A. Mittelstaedt − *Cornell University, Ithaca, New York 14850, United States*

Kaifei Kang − *Cornell University, Ithaca, New York 14850, United States*

Shengwei Jiang − *Cornell University, Ithaca, New York 14850, United States*

https://dx.doi.org/10.1021/acs.nanolett.0c02965
Nano Lett. 2020, 20, 7482−7488

Kin Fai Mak − *Cornell University, Ithaca, New York 14850, United States;* orcid.org/0000-0002-5768-199X
Jie Shan − *Cornell University, Ithaca, New York 14850, United States*
Robert A. Buhrman − *Cornell University, Ithaca, New York 14850, United States*

Complete contact information is available at: https://pubs.acs.org/10.1021/acs.nanolett.0c02965

Notes

The authors declare no competing financial interest.

■ ACKNOWLEDGMENTS

The primary source of funding for this work was the US Department of Energy (DE-SC0017671), which provided funding for V.G., who led the sample fabrication, measurements, and analysis and wrote the manuscript with D.C.R. During the final stages of the analysis and writing, support for V.G. was transferred to a new AFOSR/MURI project (FA9550-19-1-0390). T.M.C. assisted with sample fabrication and measurements, with support from the Agency for Science, Technology and Research, Singapore. Additional contributions to measurements were provided by G.M.S. (supported by DOE, DE-SC0017671), A.B. (supported by the NSF through the Cornell Center for Materials Research, DMR-1719875), and J.A.M. (supported by task 2776.047 in ASCENT, one of six centers in JUMP, a Semiconductor Research Corporation program sponsored by DARPA). K.K. (supported by the Office of Naval Research, N00014-18-1-2368.) assisted with sample fabrication, and S.J. (supported by the AFOSR/MURI, FA9550-19-1-0390) performed the MCD measurements. Sample fabrication and measurements were performed in part in the shared facilities of the Cornell Center for Materials Research and in the Cornell Nanoscale Science and Technology Facility, part of the National Nanotechnology Coordinated Infrastructure, which is supported by the NSF (NNCI-2025233).

■ REFERENCES

(1) Liu, L.; Moriyama, T.; Ralph, D. C.; Buhrman, R. A. Spin-Torque Ferromagnetic Resonance Induced by the Spin Hall Effect. *Phys. Rev. Lett.* **2011**, *106*, No. 036601.
(2) Miron, I. M.; Garello, K.; Gaudin, G.; Zermatten, P.-J.; Costache, M. V.; Auffret, S.; Bandiera, S.; Rodmacq, B.; Schuhl, A.; Gambardella, P. Perpendicular switching of a single ferromagnetic layer induced by in-plane current injection. *Nature* **2011**, *476*, 189−193.
(3) Liu, L.; Pai, C.-F.; Li, Y.; Tseng, H. W.; Ralph, D. C.; Buhrman, R. A. Spin-Torque Switching with the Giant Spin Hall Effect of Tantalum. *Science* **2012**, *336*, 555−558.
(4) Mellnik, A. R.; Lee, J. S.; Richardella, A.; Grab, J. L.; Mintun, P. J.; Fischer, M. H.; Vaezi, A.; Manchon, A.; Kim, E.-A.; Samarth, N.; Ralph, D. C. Spin-transfer torque generated by a topological insulator. *Nature* **2014**, *511*, 449−451.
(5) Fan, Y.; et al. Magnetization switching through giant spin−orbit torque in a magnetically doped topological insulator heterostructure. *Nat. Mater.* **2014**, *13*, 699−704.
(6) Han, J.; Richardella, A.; Siddiqui, S. A.; Finley, J.; Samarth, N.; Liu, L. Room-Temperature Spin-Orbit Torque Switching Induced by a Topological Insulator. *Phys. Rev. Lett.* **2017**, *119*, No. 077702.
(7) Khang, N. H. D.; Ueda, Y.; Hai, P. N. A conductive topological insulator with large spin Hall effect for ultralow power spin−orbit torque switching. *Nat. Mater.* **2018**, *17*, 808−813.
(8) Wu, H.; Zhang, P.; Deng, P.; Lan, Q.; Pan, Q.; Razavi, S. A.; Che, X.; Huang, L.; Dai, B.; Wong, K.; Han, X.; Wang, K. L. Room-Temperature Spin-Orbit Torque from Topological Surface States. *Phys. Rev. Lett.* **2019**, *123*, 207205.
(9) MacNeill, D.; Stiehl, G. M.; Guimaraes, M. H. D.; Buhrman, R. A.; Park, J.; Ralph, D. C. Control of spin−orbit torques through crystal symmetry in WTe_2/ferromagnet bilayers. *Nat. Phys.* **2017**, *13*, 300−305.
(10) Shi, S.; Liang, S.; Zhu, Z.; Cai, K.; Pollard, S. D.; Wang, Y.; Wang, J.; Wang, Q.; He, P.; Yu, J.; Eda, G.; Liang, G.; Yang, H. All-electric magnetization switching and Dzyaloshinskii−Moriya interaction in WTe_2/ferromagnet heterostructures. *Nat. Nanotechnol.* **2019**, *14*, 945−949.
(11) Li, P.; Wu, W.; Wen, Y.; Zhang, C.; Zhang, J.; Zhang, S.; Yu, Z.; Yang, S. A.; Manchon, A.; Zhang, X.-x. Spin-momentum locking and spin-orbit torques in magnetic nano-heterojunctions composed of Weyl semimetal WTe_2. *Nat. Commun.* **2018**, *9*, 3990.
(12) Gong, C.; Li, L.; Li, Z.; Ji, H.; Stern, A.; Xia, Y.; Cao, T.; Bao, W.; Wang, C.; Wang, Y.; Qiu, Z. Q.; Cava, R. J.; Louie, S. G.; Xia, J.; Zhang, X. Discovery of intrinsic ferromagnetism in two-dimensional van der Waals crystals. *Nature* **2017**, *546*, 265−269.
(13) Huang, B.; Clark, G.; Navarro-Moratalla, E.; Klein, D. R.; Cheng, R.; Seyler, K. L.; Zhong, D.; Schmidgall, E.; McGuire, M. A.; Cobden, D. H.; Yao, W.; Xiao, D.; Jarillo-Herrero, P.; Xu, X. Layer-dependent ferromagnetism in a van der Waals crystal down to the monolayer limit. *Nature* **2017**, *546*, 270−273.
(14) O'Hara, D. J.; Zhu, T.; Trout, A. H.; Ahmed, A. S.; Luo, Y. K.; Lee, C. H.; Brenner, M. R.; Rajan, S.; Gupta, J. A.; McComb, D. W.; Kawakami, R. K. Room Temperature Intrinsic Ferromagnetism in Epitaxial Manganese Selenide Films in the Monolayer Limit. *Nano Lett.* **2018**, *18*, 3125−3131.
(15) Song, T.; Cai, X.; Tu, M. W.-Y.; Zhang, X.; Huang, B.; Wilson, N. P.; Seyler, K. L.; Zhu, L.; Taniguchi, T.; Watanabe, K.; McGuire, M. A.; Cobden, D. H.; Xiao, D.; Yao, W.; Xu, X. Giant tunneling magnetoresistance in spin-filter van der Waals heterostructures. *Science* **2018**, *360*, 1214−1218.
(16) Klein, D. R.; MacNeill, D.; Lado, J. L.; Soriano, D.; Navarro-Moratalla, E.; Watanabe, K.; Taniguchi, T.; Manni, S.; Canfield, P.; Fernández-Rossier, J.; Jarillo-Herrero, P. Probing magnetism in 2D van der Waals crystalline insulators via electron tunneling. *Science* **2018**, *360*, 1218−1222.
(17) Wang, Z.; Gutiérrez-Lezama, I.; Ubrig, N.; Kroner, M.; Gibertini, M.; Taniguchi, T.; Watanabe, K.; Imamoğlu, A.; Giannini, E.; Morpurgo, A. F. Very large tunneling magnetoresistance in layered magnetic semiconductor CrI_3. *Nat. Commun.* **2018**, *9*, 2516.
(18) Jiang, S.; Li, L.; Wang, Z.; Mak, K. F.; Shan, J. Controlling magnetism in 2D CrI_3 by electrostatic doping. *Nat. Nanotechnol.* **2018**, *13*, 549−553.
(19) Liu, L.; Pai, C.-F.; Ralph, D. C.; Buhrman, R. A. Gate voltage modulation of spin-Hall-torque-driven magnetic switching. 2012, arXiv:1209.0962. arXiv.org e-Print archive.
(20) Alghamdi, M.; Lohmann, M.; Li, J.; Jothi, P. R.; Shao, Q.; Aldosary, M.; Su, T.; Fokwa, B. P. T.; Shi, J. Highly Efficient Spin−Orbit Torque and Switching of Layered Ferromagnet Fe_3GeTe_2. *Nano Lett.* **2019**, *19*, 4400−4405.
(21) Wang, X.; et al. Current-driven magnetization switching in a van der Waals ferromagnet Fe_3GeTe_2. *Science Advances* **2019**, *5*, No. eaaw8904.
(22) Ostwal, V.; Shen, T.; Appenzeller, J. Efficient Spin-Orbit Torque Switching of the Semiconducting Van Der Waals Ferromagnet $Cr_2Ge_2Te_6$. *Adv. Mater.* **2020**, *32*, 1906021.
(23) Uchida, K.-i.; Adachi, H.; Ota, T.; Nakayama, H.; Maekawa, S.; Saitoh, E. Observation of longitudinal spin-Seebeck effect in magnetic insulators. *Appl. Phys. Lett.* **2010**, *97*, 172505.
(24) Ito, N.; Kikkawa, T.; Barker, J.; Hirobe, D.; Shiomi, Y.; Saitoh, E. Spin Seebeck effect in the layered ferromagnetic insulators $CrSiTe_3$ and $CrGeTe_3$. *Phys. Rev. B: Condens. Matter Mater. Phys.* **2019**, *100*, No. 060402.
(25) Xu, J.; Phelan, W. A.; Chien, C.-L. Large Anomalous Nernst Effect in a van der Waals Ferromagnet Fe_3GeTe_2. *Nano Lett.* **2019**, *19*, 8250−8254.

(26) Fang, C.; Wan, C. H.; Guo, C. Y.; Feng, C.; Wang, X.; Xing, Y. W.; Zhao, M. K.; Dong, J.; Yu, G. Q.; Zhao, Y. G.; Han, X. F. Observation of large anomalous Nernst effect in 2D layered materials Fe_3GeTe_2. *Appl. Phys. Lett.* **2019**, *115*, 212402.
(27) Liu, T.; Peiro, J.; de Wal, D. K.; Leutenantsmeyer, J. C.; Guimarães, M. H. D.; van Wees, B. J. Spin caloritronics in a $CrBr_3$-based magnetic van der Waals heterostructure. *Phys. Rev. B: Condens. Matter Mater. Phys.* **2020**, *101*, 205407.
(28) Carteaux, V.; Brunet, D.; Ouvrard, G.; Andre, G. Crystallographic, magnetic and electronic structures of a new layered ferromagnetic compound $Cr_2Ge_2Te_6$. *J. Phys.: Condens. Matter* **1995**, *7*, 69−87.
(29) Ji, H.; Stokes, R. A.; Alegria, L. D.; Blomberg, E. C.; Tanatar, M. A.; Reijnders, A.; Schoop, L. M.; Liang, T.; Prozorov, R.; Burch, K. S.; Ong, N. P.; Petta, J. R.; Cava, R. J. A ferromagnetic insulating substrate for the epitaxial growth of topological insulators. *J. Appl. Phys.* **2013**, *114*, 114907.
(30) Lohmann, M.; Su, T.; Niu, B.; Hou, Y.; Alghamdi, M.; Aldosary, M.; Xing, W.; Zhong, J.; Jia, S.; Han, W.; Wu, R.; Cui, Y.-T.; Shi, J. Probing Magnetism in Insulating $Cr_2Ge_2Te_6$ by Induced Anomalous Hall Effect in Pt. *Nano Lett.* **2019**, *19*, 2397−2403.
(31) Avci, C. O.; Quindeau, A.; Pai, C.-F.; Mann, M.; Caretta, L.; Tang, A. S.; Onbasli, M. C.; Ross, C. A.; Beach, G. S. D. Current-induced switching in a magnetic insulator. *Nat. Mater.* **2017**, *16*, 309−314.
(32) Liu, L.; Lee, O. J.; Gudmundsen, T. J.; Ralph, D. C.; Buhrman, R. A. Current-Induced Switching of Perpendicularly Magnetized Magnetic Layers Using Spin Torque from the Spin Hall Effect. *Phys. Rev. Lett.* **2012**, *109*, No. 096602.
(33) Emori, S.; Bauer, U.; Ahn, S.-M.; Martinez, E.; Beach, G. S. D. Current-driven dynamics of chiral ferromagnetic domain walls. *Nat. Mater.* **2013**, *12*, 611−616.
(34) Zhang, C.; Fukami, S.; Sato, H.; Matsukura, F.; Ohno, H. Spin-orbit torque induced magnetization switching in nano-scale Ta/CoFeB/MgO. *Appl. Phys. Lett.* **2015**, *107*, No. 012401.
(35) Lee, O. J.; Liu, L. Q.; Pai, C. F.; Li, Y.; Tseng, H. W.; Gowtham, P. G.; Park, J. P.; Ralph, D. C.; Buhrman, R. A. Central role of domain wall depinning for perpendicular magnetization switching driven by spin torque from the spin Hall effect. *Phys. Rev. B: Condens. Matter Mater. Phys.* **2014**, *89*, No. 024418.
(36) Avci, C. O.; Garello, K.; Gabureac, M.; Ghosh, A.; Fuhrer, A.; Alvarado, S. F.; Gambardella, P. Interplay of spin-orbit torque and thermoelectric effects in ferromagnet/normal-metal bilayers. *Phys. Rev. B: Condens. Matter Mater. Phys.* **2014**, *90*, 224427.
(37) Hayashi, M.; Kim, J.; Yamanouchi, M.; Ohno, H. Quantitative characterization of the spin-orbit torque using harmonic Hall voltage measurements. *Phys. Rev. B: Condens. Matter Mater. Phys.* **2014**, *89*, 144425.
(38) Roschewsky, N.; Walker, E. S.; Gowtham, P.; Muschinske, S.; Hellman, F.; Bank, S. R.; Salahuddin, S. Spin-orbit torque and Nernst effect in Bi-Sb/Co heterostructures. *Phys. Rev. B: Condens. Matter Mater. Phys.* **2019**, *99*, 195103.
(39) Weiler, M.; Althammer, M.; Czeschka, F. D.; Huebl, H.; Wagner, M. S.; Opel, M.; Imort, I.-M.; Reiss, G.; Thomas, A.; Gross, R.; Goennenwein, S. T. B. Local Charge and Spin Currents in Magnetothermal Landscapes. *Phys. Rev. Lett.* **2012**, *108*, 106602.
(40) Schreier, M.; Roschewsky, N.; Dobler, E.; Meyer, S.; Huebl, H.; Gross, R.; Goennenwein, S. T. B. Current heating induced spin Seebeck effect. *Appl. Phys. Lett.* **2013**, *103*, 242404.
(41) Aono, T. The Nernst Effect of Bi-Sb Alloys. *Jpn. J. Appl. Phys.* **1970**, *9*, 761−767.
(42) Zhu, L.; Buhrman, R. Maximizing Spin-Orbit-Torque Efficiency of Pt/Ti Multilayers: Trade-Off Between Intrinsic Spin Hall Conductivity and Carrier Lifetime. *Phys. Rev. Appl.* **2019**, *12*, No. 051002.
(43) Li, J.; Yu, G.; Tang, C.; Liu, Y.; Shi, Z.; Liu, Y.; Navabi, A.; Aldosary, M.; Shao, Q.; Wang, K. L.; Lake, R.; Shi, J. Deficiency of the bulk spin Hall effect model for spin-orbit torques in magnetic-insulator/heavy-metal heterostructures. *Phys. Rev. B: Condens. Matter Mater. Phys.* **2017**, *95*, 241305.
(44) Guo, C. Y.; Wan, C. H.; Zhao, M. K.; Wu, H.; Fang, C.; Yan, Z. R.; Feng, J. F.; Liu, H. F.; Han, X. F. Spin-orbit torque switching in perpendicular Y $_3Fe_5O_{12}$/Pt bilayer. *Appl. Phys. Lett.* **2019**, *114*, 192409.

https://dx.doi.org/10.1021/acs.nanolett.0c02965
Nano Lett. 2020, 20, 7482−7488